A LETTERS JOURNAL EXPLORING THE FRONTIERS OF PHYSICS

OFFPRINT

Theoretical description of the nucleation of vapor bubbles in a superheated fluid

J. F. LUTSKO

EPL, **83** (2008) 46007

Please visit the new website
www.epljournal.org

TAKE A LOOK AT THE NEW EPL

Europhysics Letters (EPL) has a new online home at
www.epljournal.org

Take a look for the latest journal news and information on:

- reading the latest articles, free!
- receiving free e-mail alerts
- submitting your work to EPL

www.epljournal.org

A Letters Journal Exploring the Frontiers of Physics

August 2008

EPL, **83** (2008) 46007
doi: 10.1209/0295-5075/83/46007

www.epljournal.org

Theoretical description of the nucleation of vapor bubbles in a superheated fluid

J. F. Lutsko[(a)]

Center for Nonlinear Phenomena and Complex Systems CP 231, Université Libre de Bruxelles - Blvd. du Triomphe, 1050 Brussels, Belgium, EU

received 13 June 2008; accepted in final form 3 July 2008
published online 19 August 2008

PACS 64.60.Q- – Nucleation
PACS 64.70.F- – Liquid-vapor transitions
PACS 82.60.Nh – Thermodynamics of nucleation

Abstract – The nucleation of vapor bubbles within a superheated fluid is studied using density functional theory. The nudged elastic band technique is used to find the minimum energy pathway from the metastable uniform liquid to the stable uniform gas thus emphasizing the analogy between the the nucleation problem and that of chemical reactions. The result is both an accurate determination of the critical nucleus and an unbiased description of the density profile at various points along the path between the free energy extrema. This calculation is compared to two other methods: the use of parametrized profiles and constrained minimization of the free energy. The results indicate that the recent claim, based on the constraint method, that bubble nucleation and growth involves an activated instability is incorrect.

Copyright © EPLA, 2008

Introduction. – The process of nucleation, *e.g.* of solids from supercooled liquids or of liquids from supersaturated gases, has become the subject of intense interest in recent years driven by applications in physics, chemistry and biology. Practical problems such as the control of protein crystallization [1] have motivated experimental, theoretical and computational research which has uncovered new fundamental physics such as the important role that intermediate metastable phases may play in nucleating new phases [1–5]. In cases where this is important, nucleation becomes more complex than the simple picture of barrier crossing that underlies classical nucleation theory (CNT). Indeed, there is some theoretical evidence that the nucleation of solids from gases (a simple model of the precipitation of solids from solution) may be nonclassical even in the case of simple fluids [5]. Recently, it has even been claimed that the nucleation of gas bubbles in a superheated fluid may be nonclassical due to the presence of an "activated instability" [6].

Density functional theory (DFT) provides a natural approach to the description of nucleation. DFT is based on the fact [7,8] that the free energy is a unique functional of the local density, $\rho(\boldsymbol{r})$. In simple systems, different phases correspond to different local densities: for example, in gases and liquids, the density is a constant $\rho(\boldsymbol{r}) = \bar{\rho}$, whereas in a solid it varies over the length scale of the lattice. Nucleation can then be viewed as a process of moving from one point in density-function space to another via the most probable path. This is analogous to the usual description of a reaction pathway in a chemical system. As is usually done in chemical problems, it is natural to assume that the most probably path will be the minimum free-energy path (MFEP) so that the problem reduces to one of finding the MFEP connecting the initial and final states given the model free energy functional.

The local density is a field so that in principle its value at every point in space can vary independently giving it an infinite number of degrees of freedom. Here, attention will be restricted to spherically symmetric profiles which will furthermore be discretized on a lattice giving a finite, but still large, number of degrees of freedom. The free energy is therefore a surface in this high-dimensional space making its characterization difficult. This is analogous to the problem of characterizing reaction paths in chemical systems. Fortunately, recent years have seen the development of several sophisticated methods for addressing the problem of finding optimal pathways on high-dimensional surfaces (*i.e.*, eigenvalue following, string method, elastic band methods ...) [9]. One of the

[(a)] E-mail: jlutsko@ulb.ac.be

primary goals of this paper is to show that these methods can be applied to the description of nucleation.

Liquid-vapor nucleation in simple fluids has, of course, been studied previously and might seem too classical to warrant further effort. Although previous work has mostly focused on nucleation of droplets in a supersaturated gas, the issues are the same for droplet and bubble nucleation. Early studies [10,11] focused on the determination of the critical cluster since this is accessible (it is an extremum of the free energy) and determines the free energy barrier and, hence, the nucleation rate. In the 1990s Reiss *et al.* [12–14] developed an approximate simulation technique for studying non-critical clusters and this led to parallel theoretical developments [15] which have recently been extended to the study of gas bubbles in superheated fluids [6]. (This is referred to as the "constraint" method below.) For use in simulations, this method assumes a decoupling of clusters from the surrounding bulk. More recently, importance-sampling techniques for Monte Carlo simulations have been developed which do not depend on assumptions like decoupling [16,17]. These developments in simulation techniques are a primary motivation for the present work which aims to develop a similarly unbiased theoretical description of nucleation.

In this paper, three methods will be used to determine the properties of bubble nucleation. The simplest is the use of a parametrized profile. It is assumed that the density profile of a bubble is sigmoidal and is approximated by a generalization of a hyperbolic tangent. These profiles have two important parameters: the location of the interface, *i.e.* the bubble radius, and the width of the interface. The approximate pathway is constructed by minimizing the free energy with respect to the width of the interface for different values of the radius. The second method is the constrained optimization method originated by Talanquer and Oxtoby [15] for the study of droplet nucleation and adopted by Uline and Corti (UC) [6] for bubble nucleation where the free energy is minimized while subject to a constraint that enforces a particular bubble geometry. The third method is the nudged elastic band (NEB) [18] which is a chain of states method for constructing the MFEP. It will be shown that of the three methods, the NEB provides the most natural and reliable determination of the reaction path and that the instability identified by UC is an artifact of their method.

DFT calculations. – In DFT, the grand potential is written as

$$\beta\Omega\left[\rho\right]=\beta F\left[\rho\right]-\beta\mu\int\rho\left(\boldsymbol{r}\right)\mathrm{d}\boldsymbol{r}+\int\beta\phi\left(\boldsymbol{r}\right)\rho\left(\boldsymbol{r}\right)\mathrm{d}\boldsymbol{r},\quad(1)$$

where $\beta=1/k_BT$, μ is the chemical potential, $\phi\left(\boldsymbol{r}\right)$ is an external one-body field and $\rho\left(\boldsymbol{r}\right)$ is the local density. The functional $\beta F[\rho]$ is related to the Helmholtz free energy [8,19]. To be precise, DFT tells us that for fixed T, μ and $\phi\left(\boldsymbol{r}\right)$, the equilibrium density is a stationary point of the functional $\beta\Omega\left[\rho\right]$. In this sense, there is little direct relevance of this functional to the problem of nucleation since nucleation typically occurs at some given fixed field (either no field or the gravitational field) so that this functional can only be used to describe a few simple states: the bulk liquid and vapor and, potentially, the critical nucleus. All other intermediate states will, in general, not extremize the functional. However, it is usually assumed that at fixed field, $\beta\Omega\left[\rho\right]$ plays the role of a potential and that it can therefore be used to deduce interesting quantities such as the energy barrier for transition from one state to another.

The calculations reported here will be based on a recently developed DFT model consisting of a modified Fundamental Measure model for the short-ranged repulsion and a Van der Waals tail for the long-ranged attraction [20]. This model gives a quantitatively accurate description of the inhomogeneous Lennard-Jones liquid including the planar liquid-vapor interface, the liquid near a wall and the liquid confined to a slit pore. The bulk thermodynamics was approximated using the empirical 33-parameter equation of state of Johnson, Zollweg and Gubbins [21].

Three methods are used to explore the free energy landscape. The first and simplest is the use of a parametrized profile. The parametrization used here is a modified hypertangent,

$$\rho\left(r\right)=\rho_l+\left(\rho_v-\rho_l\right)\frac{1+br}{1+\left(br\right)^2}\frac{1-\tanh\left(A(r-R)\right)}{1-\tanh\left(-AR\right)}\quad(2)$$

with

$$b=\frac{2A}{e^{2AR}+1}.\quad(3)$$

and where ρ_l (ρ_v) is the density of the bulk liquid (vapor) for the given temperature and chemical potential. This function is constructed so that at it approaches ρ_l as $1/r$ at large distances while also satisfying $\mathrm{d}\rho/\mathrm{d}r\to0$ as $r\to0$. In the calculations presented below, the free energy is minimized with respect to the width parameter A for fixed values of the radius, R.

The second method used was the constraint method of Talanquer and Oxtoby [15] as adapted by Uline and Corti [6]. Here, one characterizes a bubble by some property of the density which can be written schematically as $g\left(\left[\rho\right],\Gamma\right)=0$ where the notation indicates that the left-hand side is a functional of the local density and that it also depends on one or more parameters denoted collectively as Γ. Different values of the parameters correspond to bubbles having different properties (mass, radius, ...). It is assumed that for fixed parameters, the most energetically accessible structure is that which minimizes the free energy subject to the structural constraint. This is implemented via a Lagrange multiplier by extremizing the functional $\beta\Omega\left[\rho\right]-\alpha g\left(\left[\rho\right],\Gamma\right)$ giving the equations

$$\frac{\delta\beta F\left[\rho\right]}{\delta\rho\left(\boldsymbol{r}\right)}-\beta\mu-\alpha\frac{\delta g\left(\left[\rho\right],\Gamma\right)}{\delta\rho\left(\boldsymbol{r}\right)}=0\quad(4)$$

and $g([\rho],\Gamma)=0$. In this picture, the role of the constraint is to reduce the number of degrees of freedom from an essentially infinite number needed to describe all possible density functionals to a few, the collection of parameters Γ, which then define a path from the uniform liquid to the uniform vapor. The question then is what to use for the structural constraint. First, note that if there is no structural constraint, then the uniform state satisfies the usual thermodynamic relation $\frac{\partial V f(\rho)}{\partial \rho}=\mu$, where $f(\rho)$ is the bulk free energy per unit volume, and there are two solutions corresponding to the uniform vapor, ρ_v, and liquid, ρ_l, states. Perhaps the most natural choice for the constraint is the number of atoms "missing" from the bubble relative to the liquid background,

$$g([\rho],\Gamma)=\int(\rho_l-\rho(\boldsymbol{r}))\,\mathrm{d}\boldsymbol{r}-\Delta N, \tag{5}$$

where ΔN is the desired deficit. In this case, the only parameter is $\Gamma=\Delta N$. However, substitution into eq. (4) shows that this changes the chemical potential from μ to $\mu+\alpha$ so that the liquid density far from the bubble would necessarily be incorrect. This seems to indicate that a localized bubble can only be described by a constraint that vanishes at large r. UC therefore propose

$$g_{UC}([\rho],\Gamma)=\int\Theta(\lambda-r)\,\rho(r)\,\mathrm{d}\boldsymbol{r}-N, \tag{6}$$

where $\Theta(x)$ is the step function and there are two parameters, the "radius" λ and the total number of atoms in the bubble, N [6]. (For the reverse problem of droplet nucleation, Talanquer and Oxtoby also use this constraint but they say they adjust the bulk outside the volume in a way which appears to imply the use of eq. (5) [15].) UC show that, for a fixed value of N, solutions only exist for λ less than some critical value and this is interpreted as indicating that bubbles of larger size are unstable. I propose here another constraint that is based on defining the size a bubble implicitly as the position at which the density becomes greater than some value, ρ_*,

$$g_*([\rho],\Gamma)=\int\Theta(\rho(r)-\rho_*)\,\mathrm{d}\boldsymbol{r}-\Gamma. \tag{7}$$

This is physically appealing and is also similar to a criterion used to define clusters in some computer simulations [16]. In this case there are in principle two parameters: Γ, which is a measure of the volume of the bubble, and ρ_* which will be taken to be $\frac{1}{2}(\rho_l+\rho_v)$.

Finally, the third method used is the nudged elastic band [18]. These calculations begin with some number, N, of density profiles corresponding to eq. (2) with values of R spaced evenly from $R=0$ to some R_{max}. The various profiles represent points along a path from the initial state (the uniform fluid corresponding to $R=0$ in eq. (2)) to the final state which here is taken to be again a sigmoidal with a fixed, large radius and optimized width. (These endpoints remain fixed during the calculation and the remaining images are referred to as "moveable".) Unlike the first method, each of these images are not restricted to be given by the parametrized form of eq. (2) but is instead a discretized density profile, $\rho(r_i)$, that can assume any shape. If the sum of the free energies of all of the moveable profiles was minimized, the final result would be that each profile would tend toward one of the minima —either the uniform liquid or the uniform vapor, depending on the starting point. To avoid this, the NEB involves two elements. First is the addition of artificial elastic forces between neighboring profiles so that the images are forced to be more or less uniformly distributed along the MFEP. To define the elastic forces, the distance between two profiles was defined to be

$$|\rho_1-\rho_2|^2=\int w(r)\,(\rho_1(\boldsymbol{r})-\rho_2(\boldsymbol{r}))^2\,\mathrm{d}\boldsymbol{r}. \tag{8}$$

The definition allows for a weight, $w(r)$, since there are at least two natural choices one could make in a spherical geometry. The first is, of course, $w(r)=1$, while the second is $w(r)=r^{-2}$. For spherically symmetric density distributions, the first choice has the effect of giving more weight to differences in density at large r than at small distances while the second weights all radial points equally. Calculations were performed using both definitions and it was found, as shown below, that the choice had no effect on the final results except for affecting the relative spacing of the images along the MFEP: the second choice gives more images at small r than the first choice but the path so defined was virtually identical.

The second element of the NEB method is that this combination of the free energies and artificial elastic forces is minimized under the constraint that the elastic forces only act along the MFEP and the force arising from the free energies act only perpendicular to the MFEP (the "nudging"). This method is not guaranteed to give the exact MFEP but it has proven a useful heuristic in numerous applications. A further modification involves choosing one image and forcing it to climb the gradient along the MFEP without any spring forces [22]. This gives a very accurate and convenient characterization of the saddle point. The relaxation of the system of images and harmonic forces was performed using the fast inertial relaxation engine algorithm [23].

Results. – The three methods were compared for the case of a Lennard-Jones potential, $V(r)=4\epsilon\left(\left(\frac{\sigma}{r}\right)^{12}-\left(\frac{\sigma}{r}\right)^{6}\right)$ witha cutoff at $r=4\sigma$. The calculations reported here were performed at a reduced temperature $k_BT/\epsilon=0.8$ and the chemical potential was fixed at 10% below coexistence corresponding, roughly, to the state conditions used by UC [6]. The densities of the coexisting liquid and vapor were found to be $\rho_l\sigma^3=0.784$ and $\rho_v\sigma^3=0.008$, respectively.

Figure 1 shows the excess free energy, calculated using all three methods, as a function of the size of the bubble as quantified by the number deficit (*i.e.* as defined via

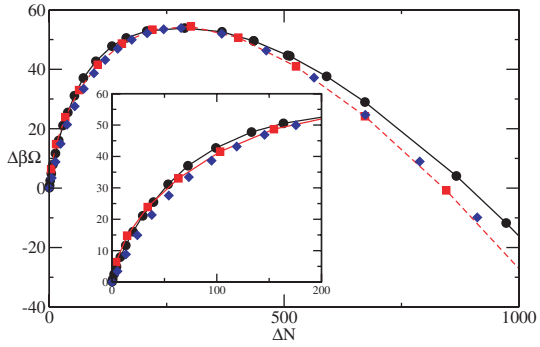

Fig. 1: (Color online) Excess free energy as a function of the atomic deficit as calculated using DFT with the proposed structural constraint given in eq. (7), circles and solid line, using a modified hyperbolic tangent profile, eq. (2), squares and broken lines, and the NEB method, diamonds.

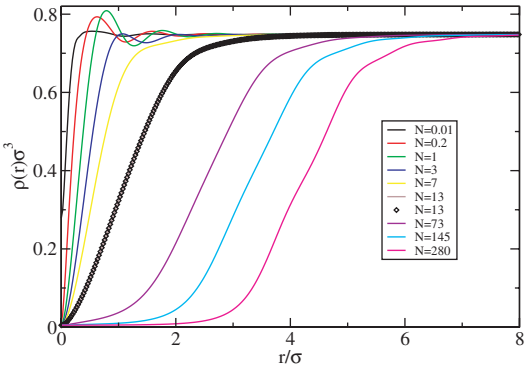

Fig. 2: (Color online) Structure of small bubbles along the MFEP as determined using the NEB method. Structures up to $N = 13$ were calculated using the metric with $w(r) = r^{-2}$ weight whereas structures for $N = 13$ and larger were performed including the $w(r) = 1$. The $N = 13$ structure is shown as calculated both ways (line is without the weight and the symbols are with the weight) illustrating the insensitivity of the calculation to the weight used in the metric.

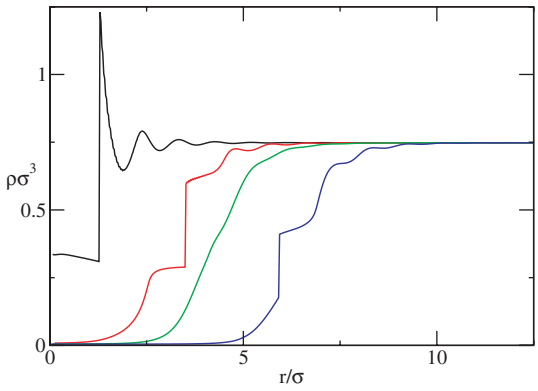

Fig. 3: (Color online) Density profiles for several different bubble sizes of, from left to right, $\Delta N = 4$, 163, 288 and 866 as calculated using the constraint method.

eq. (5)). The constraint method has been implemented using eq. (7). All three methods are in close agreement for the height of the free-energy barrier and the size of the critical cluster. However, away from the critical cluster, the constraint method gives systematically higher free energies than do the other two methods. For the initial part of the bubble formation, from the uniform fluid to the critical cluster, the NEB method gives the lowest free energies and, hence, is closest to the MFEP. For bubbles larger than the critical cluster, the NEB energies are very close to, but slightly higher than, those calculated using the parametrized profile. This is probably due to the fact that the end point of the chain of states used in the NEB calculation is not the uniform gas —since the uniform gas is a bubble of infinite size, it cannot serve as the end of the chain— but, rather, a parametrized profile which thus distorts the NEB chain away from the MFEP.

Figure 2 shows the density profiles calculated using the NEB method. The bubble initially forms as a small drop in the density very close to the origin. The central density quickly becomes that of the coexisting gas but the bubble is still very small due to the fact that the interface is extremely narrow. At this stage, some structure forms in the liquid which is similar to that seen in a fluid near a hard wall [20]. The bubble grows via the broadening of the interface and as the interface broadens, the liquid structure vanishes. Only when the interface is sufficiently broad, in this case, when the number deficit is about 70 atoms or so, does a recognizable sigmoidal structure develop. Further growth consists of a displacement of the interface with little change in structure.

When the free energy is minimized for a spherically symmetric density profile with the UC constraint, the results of UC are reproduced: namely, for fixed N, there is a maximum value of the radial parameter, λ, beyond which no stable profile exists. The physics of this apparent instability will be the subject of the next section.

Using the proposed constraint, a different picture emerges. It is possible to stabilize the density profile for all values of the parameter Γ. For each value of Γ, the total atomic deficit can be calculated and the resulting free-energy curve is shown in fig. 1 which confirms the CNT picture and shows no sign of an instability. However, because the constraint has the effect of shifting the chemical potential inside the bubble, but not outside, (see eq. (4)), the profiles generated are discontinuous, as can be seen in fig. 3. The only continuous profile obtained is for the special case of the critical nucleus, for which the Lagrange multiplier α is zero. The discontinuity of the profiles is responsible, at least in part, for the higher free energies calculated for this model as shown in fig. 1.

Illustration on a simple model. – It is useful to consider a simple, but instructive, analytic model for which it is possible to see why the constraint method can give instabilities. Consider the square-gradient model first

introduced by van der Waals [24,25],

$$\beta F[\rho] = \int \left[\beta f(\rho(r)) + \frac{1}{2}\tau \left(\frac{\partial \rho(r)}{\partial r} \right)^2 \right] \mathrm{d}\boldsymbol{r}, \quad (9)$$

where again $f(\rho)$ is the free energy per unit volume of the uniform fluid and where the constant τ is called the accommodation factor. This model is not quantitatively very accurate, but it is a systematic approximation to more realistic models and is still often used in the literature. Combined with the structural constraint, this can be used to determine the density. The problem is simplified if one uses a parametrized density and here I consider a very simple piecewise linear approximation,

$$\rho(r) = \begin{cases} \rho_0, & r < R, \\ \rho_0 + \frac{\rho_\infty - \rho_0}{w}(r - R), & R < r < R + w, \\ \rho_\infty, & R < r. \end{cases} \quad (10)$$

Potentially, the width, w, the bubble density, ρ_0, the outer density, ρ_∞ and radius R are determined by minimizing the grand potential (with the structural constraint). For the outer density, this gives $\rho_\infty = \rho_l$. However, for the remaining parameters, this is still too complicated, so I consider the simplest case that the width goes to zero. If this limit is take, while holding $\gamma \equiv \tau/w$ constant, then the resulting functional using the UC constraint is easily shown to be

$$\begin{aligned} &\beta\Omega[\rho] - \alpha g_{UC}([\rho], \Gamma) = \\ &\frac{4\pi}{3} R^3 \{ f(\rho_0) - f(\rho_l) - \mu(\rho_0 - \rho_l) \} \\ &-\alpha \begin{Bmatrix} +4\pi\gamma R^2 (\rho_l - \rho_0)^2 \\ \left(\frac{4\pi}{3}\lambda^3 \rho_0 - N \right) \Theta(R - \lambda) \\ + \left(\frac{4\pi}{3} R^3 \rho_0 + \frac{4\pi}{3}(\lambda^3 - R^3)\rho_l - N \right) \Theta(\lambda - R) \end{Bmatrix}. \end{aligned} \quad (11)$$

Notice that in the absence of the constraint, $\alpha = 0$, this is the usual functional assumed in classical nucleation theory if one takes $\rho_0 = \rho_v$. In that case, the free energy is a function of a single parameter, the radius R, and it is easy to see that $\beta\Omega[\rho]$ as a function of R shows a minimum at $R = 0$ (the liquid) a maximum at some finite value of R and a monotonic decrease for larger values of R. This is just the CNT picture of nucleation as a process of thermally activated barrier crossing. Using the proposed constraint, the functional to be minimized is the same as the UC functional except the Lagrange multiplier term is $-\alpha\left(\frac{4\pi}{3}R^3 - \Gamma\right)$, provided that $\rho_0 < \rho_* < \rho_l$.

The difficulties of the UC model become apparent when the free energy is minimized with respect to the free parameters of the density profile. There are two cases depending on whether R or λ is larger. Minimizing under the assumption $0 < R < \lambda$ gives

$$\begin{aligned} R &= \frac{4\gamma(\rho_l - \rho_0)^2}{f(\rho_0) - f(\rho_l) - f'(\rho_0)(\rho_0 - \rho_l)}, \\ R^3\rho_0 &= \frac{3}{4\pi}N - \left(\lambda^3 - R^3\right)\rho_l. \end{aligned} \quad (12)$$

Now, consider what happens when λ becomes large and N is held fixed. Since $\rho_0 > 0$, it follows that $R^3 > \lambda^3 - \frac{3}{4\pi\rho_l}N$, which means that $R \sim \lambda$. This in turn implies that $\rho_0 < \frac{3}{4\pi R^3}N \sim \frac{3}{4\pi\lambda^3}N$, so that the central density tends to zero. However, at small ρ_0, one has that $f(\rho_0) = \rho_0 \ln\rho_0 - \rho_0 + O\left(\rho_0^2\right)$ giving

$$R = \frac{4\gamma\rho_l^2 + O(\rho_0)}{\rho_l \ln\rho_0 - f(\rho_l) + O(\rho_0)} \quad (13)$$

and this is clearly negative for sufficiently small ρ_0, that is to say for sufficiently large λ. Since the radius must be positive, this is unphysical. The alternative, $R > \lambda$, leads to

$$\begin{aligned} R &= -\frac{2\gamma(\rho_l - \rho_0)^2}{f(\rho_0) - f(\rho_l) - \mu(\rho_0 - \rho_l)}, \\ \rho_0 &= \frac{3}{4\pi\lambda^3}N. \end{aligned} \quad (14)$$

Again, the central density tends to zero as λ becomes large. In this case, one has that

$$\lim_{\rho_0 \to 0} R = -\frac{2\gamma{\rho_l}^2}{-f(\rho_l) + \mu\rho_l} = -\frac{2\gamma{\rho_l}^2}{\beta P(\rho_l)}, \quad (15)$$

where $P(\rho_l)$ is the pressure of the bulk liquid. It is evident that the radius again becomes negative thus violating the assumption that $R > \lambda$. There is therefore no nontrivial solution for large λ, which is exactly the conclusion of UC. However, in this case the underlying free energy is clearly well defined for all bubbles (*i.e.* for all values of ρ_0 and R) so that the lack of solution is a statement about the structural constraint and tells us nothing about the free energy of bubbles.

It might seem that the pathology of this model is due to the extremely simplified density profile. However, a look at the proposed structural constraint shows that this is not necessarily the case. In fact, minimization of the free energy with respect to the Lagrange multiplier, α, and the central density, ρ_0, gives $\Gamma = \frac{4\pi}{3}R^3$ and

$$f'(\rho_0) = \mu - \frac{3\gamma(\rho_l - \rho_0)^2}{R}. \quad (16)$$

The first relation shows a simple one-to-one relation between the parameter Γ and the bubble radius while the second relation serves to fix the central density. For large radii, that density tends to the density of the bulk gas. For small radii, taking into account that the chemical potential for a gas is generally negative and that $f'(\rho_0) \sim \log(\rho_0)$,

it is clear that the central density tends to zero. There is a third relation that results from minimizing with respect to R but this serves to fix the Lagrange multiplier and is of no particular interest. Finally, note that these conclusions are independent of the value of ρ_* provided it lies in the range $[\rho_v, \rho_l]$.

This analysis is consistent with the more detailed calculations of the previous section and shows that the lack of existence of a density profile that minimizes the constrained free energy does not necessarily mean that the unconstrained free energy is pathological in any way. In the present case, the CNT free energy is a well-behaved function of the local density (characterized by the parameters ρ_0, ρ_∞ and R).

Conclusions. – The MFEP for bubble formation in a superheated liquid was calculated using three different methods. The most robust method appears to be the NEB. In this approach, no *a priori* assumptions are made about the structure of bubbles and the results were found to be robust with respect to the metric used and the choice of parameters. The method yields a well-defined picture of bubble formation and growth that is broadly consistent with that of classical nucleation theory.

It is perhaps surprising that the use of parametrized profiles appears to be almost as good as the NEB method in terms of the description of the critical cluster as well as the calculation of the free energy as a function of number deficit. For very small bubbles, the assumption of a sigmoidal shape is not correct, but the free energy is relatively insensitive to this error since, in a spherical geometry, the characteristic r^2 weighting in the integrals minimizes the contribution of the structure near the origin while larger bubbles actually are sigmoidal.

The constraint method gave the worst results. In particular, it is not robust: the use of the UC constraint only gives nontrivial results for small bubbles whereas the alternative constraint discussed here gives stable profiles of all sizes. In both cases, the profiles are discontinuous except for the critical cluster thus giving a higher free energy than the other methods. The failure of the UC constraint to stabilize large bubbles was analyzed using a simple model and it was shown that the apparent instability was an artifact of the constraint method and tells nothing about the underlying free-energy surface.

The conclusion, based on the combination of numerical calculations and analysis of a simple model presented here, is that bubble nucleation and growth does not involve an "activated instability" as previously claimed [6] but, rather, appears to follow the picture, if not the details, of classical nucleation theory rather well.

* * *

I am grateful to G. Nicolis for encouragement and for several useful comments on this work. This work was supported in part by the European Space Agency under contract No. ESA AO-2004-070.

REFERENCES

[1] Vekilov P. G., *Crys. Growth Des.*, **4** (2004) 671.
[2] ten Wolde P. R. and Frenkel D., *Science*, **77** (1997) 1975.
[3] Talanquer V. and Oxtoby D. W., *J. Chem. Phys.*, **109** (1998) 223.
[4] Shiryayev A. and Gunton J. D., *J. Chem. Phys.*, **120** (2004) 8318.
[5] Lutsko J. F. and Nicolis G., *Phys. Rev. Lett.*, **96** (2006) 046102.
[6] Uline M. J. and Corti D. S., *Phys. Rev. Lett.*, **99** (2007) 076102.
[7] Mermin N. D., *Phys. Rev.*, **137** (1965) A1441.
[8] Hansen J.-P. and McDonald I., *Theory of Simple Liquids* (Academic Press, San Diego, Cal.) 1986.
[9] Wales D., *Energy Landscapes* (Cambridge University Press, Cambridge) 2003.
[10] Lee D. J., da Gama M. M. T. and Gubbins K. E., *J. Chem. Phys.*, **85** (1986) 490.
[11] Oxtoby D. W. and Evans R., *J. Chem. Phys.*, **89** (1988) 7521.
[12] Reiss H., Tabazadeh A. and Talbot J., *J. Chem. Phys.*, **92** (1990) 1266.
[13] Ellerby H. M., Weakliem C. L. and Reiss H., *J. Chem. Phys.*, **95** (1991) 9209.
[14] Weakliem C. L. and Reiss H., *J. Chem. Phys.*, **99** (1993) 5374.
[15] Talanquer V. and Oxtoby D. W., *J. Chem. Phys.*, **100** (1994) 5190.
[16] Rien ten Wolde P. and Frenkel D., *J. Chem. Phys.*, **109** (1998) 9901.
[17] Frenkel D. and Smit B., *Understanding Molecular Simulation* (Academic Press Inc., Orlando, Fla.) 2001.
[18] Henkelman G. and Jónsson H., *J. Chem. Phys.*, **113** (2000) 9978.
[19] Evans R., *Adv. Phys.*, **28** (1979) 143.
[20] Lutsko J. F., *J. Chem. Phys.*, **128** (2008) 184711.
[21] Johnson J. K., Zollweg J. A. and Gubbins K. E., *Mol. Phys.*, **78** (1993) 591.
[22] Henkelman G., Uberuaga B. P. and Jónsson H., *J. Chem. Phys.*, **113** (2000) 9901.
[23] Bitzek E., Koskinen P., Gahler F., Moseler M. and Gumbsch P., *Phys. Rev. Lett.*, **97** (2006).
[24] van der Waals J. D., *Z. Phys. Chem.*, **13** (1894) 657.
[25] Rowlinson J. S., *J. Stat. Phys.*, **20** (1979) 197.